Journal of GeoEngineering, Vol. 16, No. 4, pp. 121-131, December 2021
http://dx.doi.org/10.6310/jog.202112_16(4).1

BEHAVIOR OF APPARENT DISPERSION CURVE AND ITS IMPLICATION TO MASW TESTING

Chih-Ping Lin [1*], Almira Sufwandini Putri [2], Tsai-Jung Wu [3], and Ernian Pan [4]

ABSTRACT

Despite their efficiency and usefulness in geotechnical engineering, the un-standardized surface wave methods are still limited in certain aspects. Among these methods, the MASW (multi-station analysis of surface wave) is the more popular one nowadays. The MASW is mainly based on picking the fundamental-mode dispersion curve for shear-wave velocity inversion. However, the fundamental mode may not always dominate. This study investigates specifically under what condition and how higher modes may affect the apparent dispersion curves, *i.e.,* apparent from dispersion analysis of seismic recordings. Four simplified yet distinct types of shear-wave velocity profiles were used to examine the experimental dispersion characteristics in relation to their theoretical modal dispersion curves. When there is an embedded layer which is softer than the surface layer, the dominant mode jumps to higher modes at wavelength greater than the bottom depth of the soft layer. As the soft layer moves deeper, the information contained in the fundamental-mode inversion is reduced. The transition between different modes may be smooth and the apparent dispersion curve may appear as a single mode. When multiple modes do separate, there is no fixed pattern as to which higher mode would dominate the sequence of mode jumping. Therefore, definite assignment of mode numbers in multi-mode inversion is unlikely. This study not only reveals this potential pitfall, but also shows remarkable difference in dispersion images and patterns of dominant higher modes in response to different velocity profiles. A modified simplified inversion can correctly detect the embedded soft layer and the type of velocity profile, but the accuracy is not always good. More rigorous inversion based on the apparent dispersion curve or dispersion spectrum is imperative to further improve the reliability of the MASW method.

Key words: Surface wave, dispersion curve, multi-channel analysis of surface wave (MASW), spectral analysis of surface wave (SASW).

1. INTRODUCTION

Seismic surface wave method, which is based on phase-velocity dispersion in response to vertical variation of shear-wave velocity, is one of the most relevant geophysical methods in geotechnical engineering. It provides estimation of ground stiffness (in terms of shear modules or shear-wave velocity) in a non-invasive manner with a large sample volume. It has been an efficient tool for assessing soil dynamic properties, soil liquefaction, soil-structure interaction, and static deformation (Tokimatsu 1995; Lin *et al.* 2004; Di Benedetto *et al.* 2003; Stokoe *et al.* 2004). Although the shear modulus derived from the seismic surface wave method is a small-strain elastic measurement, non-destructive in-situ measurement of small-strain modulus is a critical component in predicting the non-linear stress-strain relation in the field (Stokoe *et al.* 2004). Nonetheless, many geotechnical practitioners are still not confident to replace down-hole seismic (or down-hole CPT) and cross-hole seismic methods with the surface wave method. This is partly due to the non-uniqueness nature in geophysical methods and the lack of standard for the surface wave method.

All seismic surface wave methods involve three distinct steps: (1) field testing to acquire time and space-sampled surface waves (typically the Rayleigh waves); (2) signal processing to obtain dispersion curve from field data; and (3) inversion for shear-wave velocity (V_S) from the apparent dispersion curve. Different variants of surface-wave methods take different approaches in one or more of these three steps. Among these methods, Spectral Analysis of Surface Waves (SASW) (Heisey *et al.* 1982; Joh 1996) and Multi-channel Analysis of Surface Waves (MASW) (Park *et al.* 1999; Xia *et al.* 1999) are the two major iconic approaches with more of geotechnical and geophysical inheritance, respectively. The SASW method was developed much earlier requiring only two receivers and a two-channel dynamic analyzer. It is not possible to identify different propagation modes with only two-station data; hence the obtained phase velocity of each frequency component is deemed apparent when there are multiple modes. With the advancement of hardware and signal processing techniques, the MASW method was later proposed taking advantage of the multi-station data, from which different propagation modes can be identified by wavefield transformation. That is, distinct phase velocities corresponding to different propagation modes can be identified if the space window of the wavefield is sufficiently large (Lin and Chang 2004).

Manuscript received March 17, 2021; revised July 26, 2021; accepted September 17, 2021.
[1*] Professor (corresponding author), Department of Civil Engineering, National Yang Ming Chiao Tung University, 1001 Ta-Hsueh Rd., Hsinchu 300, Taiwan (e-mail: cplin@mail.nctu.edu.tw).
[2] M.S. Graduate, Department of Civil Engineering, National Yang Ming Chiao Tung University, 1001 Ta-Hsueh Rd., Hsinchu 300, Taiwan.
[3] Ph.D. Candidate, Department of Civil Engineering, National Yang Ming Chiao Tung University, 1001 Ta-Hsueh Rd., Hsinchu 300, Taiwan.
[4] Professor, College of Engineering, Cleveland State University, Cleveland, Ohio, U.S.A.

A detailed comparison of these two methods in terms of dispersion analysis was reported (Lin *et al.* 2017). The two methods also differ in the inversion step. Due to the apparent nature of the dispersion analysis, the SASW method emphasizes the inversion based on computation of apparent dispersion curve, which is more computationally involved than the fundamental-mode dispersion curve (Joh 1996; Ganji *et al.* 1998). On the contrary, with the capability of distinguishing multiple modes, the MASW method is mainly based on the fundamental-mode inversion and optionally multiple-mode inversion (Xia *et al.* 2003). The apparent dispersion curve has to be computed from the dynamic response, while theoretical modal dispersion curve is derived from a characteristic equation corresponding to the free vibration without actually solving for the dynamic response. The MASW method is gaining popular in practice due to its efficient, robust, and objective dispersion analysis with intuitive dispersion visualization, as well as efficiency in the inversion analysis. However, many MASW testing results revealed that clear fundamental mode may not be obtained or separated from higher modes in some frequency range. The resolution of dispersion spectrum image depends on the receiver spread length (Lin and Chang 2004). More importantly, dominance of higher modes may take place depending on the earth profile. It has been pointed out that higher modes may dominate at higher frequencies in inverse velocity profiles or when there are embedded soft layers, while the fundamental mode generally dominates across all frequencies in regular velocity profiles where shear wave velocity increases with depth (Lucena and Taioli 2014; Lu *et al.* 2015). Although there has been a general understanding of possible higher modes, it is not clear exactly when and how higher modes would dominate. Thus, the objective of this study is to investigate the behavior of the surface wave dispersion in the context of MASW testing. The dispersion characteristics observed from the finite-length MASW data are examined and compared with the theoretical modal dispersion curves for different types of earth profiles. The implications of the dispersion behavior on MASW data inversion are thoroughly discussed in this study.

2. METHODS

To explore the behavior of the surface-wave dispersion, a few synthetic models for dynamic response simulation are set, so that the ground truth is known. These synthetic models are simplified yet very different and typical earth velocity profiles. This allows us to capture the behavior pattern of the apparent dispersion curve. As illustrated in Fig. 1, these representative models include: (a) normal profile (increasing velocity with depth); (b) inverse profile (decreasing velocity with depth); (c) velocity profile; and (d) complex velocity profile. The complex velocity profile type (Fig. 1(d)) is frequently encountered in the field where a stiffer surface layer exits due to soil desiccation. There are totally sixteen synthetic models derived from these four types of velocity profiles with different velocity variations. When performing dynamic response and modal dispersion curve analyses, the Poisson's ratio was fixed at 0.33 and the typical densities corresponding to the stiffness were used. Since the surface wave dispersion is dominated by the shear wave velocity (V_S), Fig. 1 and later figures show only the shear wave velocity profiles for simplicity.

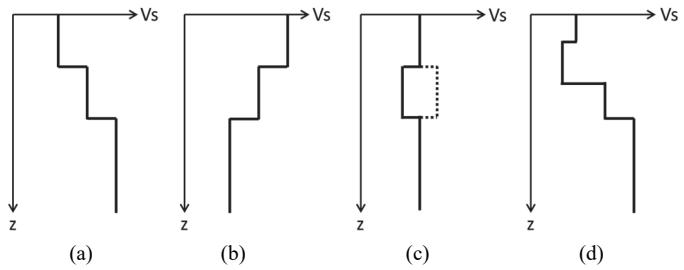

Fig. 1 Four types of velocity profiles investigated: (a) normal velocity profile; (b) inverse velocity profile; (c) velocity profile; and (d) complex velocity profile

Different definitions of dispersion curves are first clarified. Given the velocity profile of a layered medium, the wave equation leads to a characteristic equation, in which multiple possible roots of phase velocity (V_{ph}) (or wavenumber) can be found for each frequency. These solutions are the modal dispersion curves, in which the fundamental mode is the solution with the lowest $V_{ph}(f)$, and roots of higher phase velocities are higher modes. Different modes may contribute, to some degree, to the actual dynamic response. The actual participating modes in a dynamic response can be revealed from the acquired multi-station wavefield data using a wavefield transformation to be explained later. Ideally, it is possible to obtain the contribution percentage of each participating mode if the complete lossless wavefield can be captured. However, due to limited number of geophones and wave attenuation, only a truncated version of the complete wavefield is experimentally acquired. The peaks of the frequency-phase velocity spectrum in the wavefield transformation correspond to the effective or apparent dispersion curve. The apparent dispersion curve is surely governed by the velocity profile of the layered medium, but also affected by the location and size of the geophone array. This study is aimed at scrutinizing the behavior of apparent dispersion curve in relation to theoretical modal dispersion curves and velocity profiles.

2.1 Theoretical Modal Dispersion Curves

Two popular methods for determining the modal dispersion curves of a horizontally layered medium are the transfer matrix method (Thomson 1950; Haskell 1953) and global stiffness matrix method (Kausel and Roesset 1981). The more stable stiffness matrix method was adopted in this study. For a horizontally layered medium, as shown in Fig. 2, and assuming axial symmetric motion (*i.e.,* ground motion subjected to a circular vertical loading), the element stiffness matrix, which relates the tractions and displacements at the upper and lower interfaces of the layer, can be derived from the general solution of wave equation in the frequency (ω) and wavenumber (k) domain (Kausel and Roesset 1981). In a manner similar to the finite element method, the element stiffness matrix can be assembled into a global stiffness matrix [$\boldsymbol{K}$], relating the nodal forces to the nodal displacements at the layer interfaces. The natural (free) modes of the Rayleigh wave are obtained by considering a system without external loading (*i.e.,* zero force vector). To obtain the non-trial solution, the determinant of the global stiffness matrix [$\boldsymbol{K}(\omega, k)$] has to be zero. For a given frequency, the value of the wavenumber, and hence the phase velocity $V_{ph} = \omega/k$, can be determined by setting the determinant of global

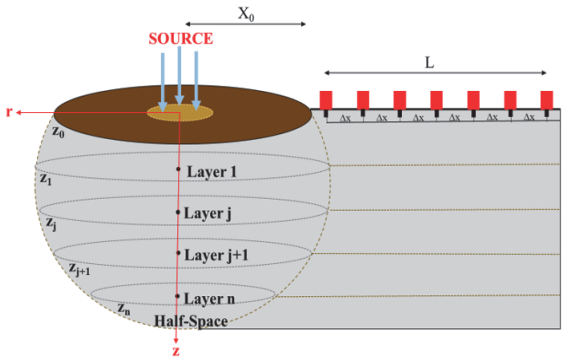

Fig. 2 Illustration of dynamic response in a horizontally layered medium and MASW field testing layout

stiffness matrix equal to zero. This is basically a root finding problem. Different wavenumbers (or phase velocities) determined at a given frequency correspond to dispersion curves with different modes. For instance, the largest wavenumber, hence the lowest phase velocity, for a given frequency belongs to the fundamental mode of the theoretical modal dispersion curves; the second largest wavenumber belongs to the first higher mode of the theoretical modal dispersion curves (for simplicity, fundamental mode and i^{th} higher mode will be used to indicate the fundamental mode and i^{th} higher mode of theoretical modal dispersion curves, respectively). An open-source software, MASWaves (Olafsdottir *et al.* 2018), contains a function (MASWaves_theoretical_dispersion_curve.m) for computing the fundamental-mode dispersion curve in terms of the wavelength *vs.* phase velocity. This function was modified to include solutions for higher modes and to present the dispersion curves in terms of frequency *vs.* phase velocity.

2.2 Dynamic Response

While the dispersion relation is obtained by setting a zero traction condition at the surface (*i.e.,* corresponding to free vibration) and finding the roots of the characteristic equation (*i.e.,* determinant of [***K***] equals to 0), the dynamic response is determined by setting the loading boundary condition and solving for the induced displacements or stresses. Finding the modal dispersion curves is much faster than computing the dynamic response subjected to a circular loading. However, in order to investigate the behavior of the field apparent dispersion curve, accurate dynamic response of the actual wavefield is needed. Normally in complex 2D or 3D conditions, finite element or finite difference methods are often used for such simulations. For a horizontally-layered system, complete analytical solutions can be found in the frequency-wavenumber domain, and numerical integration or transformation can be used to calculate the dynamic response in the time-space domain (Kausel and Roesset 1981; Roesset and Shao 1985; Al-Khoury *et al.* 2001; Liu and Pan 2018). This gives the synthetic data for MASW testing illustrated in Fig. 2. For this study, our objective is to investigate the dispersion behavior in the frequency domain. Therefore, only the frequency response is required (*i.e.,* the seismic source illustrated in Fig. 2 is a time-harmonic loading proportional to $e^{i\omega t}$). This is equivalent to the Fourier transform of the field data subject to an impact loading. In this manner, we save the inverse transform computation of the wavefield from frequency to time domain.

In order to compute the frequency response at the designated receiver locations, as illustrated in Fig. 2, the dynamic version of a layered elastic analysis (LEA) code called MultiSmart3D (*e.g.,* Alkasawneh *et al.* 2007; Liu and Pan 2018) was used. It is based on a novel cylindrical system of vector functions combined with a new propagation matrix method called DVP (dual variable and position method). The DVP algorithm involved has been thoroughly validated for its accuracy and efficiency in both engineering and science fields (Liu *et al.* 2018; Liu and Pan 2018; Zhou *et al.* 2021). While the dynamic MultiSmart3D is capable of dealing with layered, transversely isotropic and elastic half-spaces with imperfect interfaces, we assumed isotropic and perfect interface conditions in this study, which are also the current practice in the MASW method. The same material properties (layer thickness, V_S, V_P, and density) in the previous section for the theoretical dispersion curves were used for computing the frequency response. The receiver locations for computing dynamic responses are based on the recommended field parameters by Park and Carnevale (2010). With about 30 m of maximum investigation depth and 48 available channels in mind, 24 m near offset (distance between the source to the closest receiver) and 1 m receiver spacing were used for computing the frequency responses at the 48 receiver locations. Although the actual testing configuration may be adjusted depending on the field condition, this fixed receiver array is representative for investigating the behavior of the apparent dispersion relation. An example of the frequency response (vertical component as in a typical MASW testing in which vertical geophones are used) is shown in Fig 3(a), in which the real and imaginary parts of the frequency response oscillate and attenuate gradually with the distance from the source. This oscillation with distance is purely harmonic if there is only one mode, and the oscillation period in space corresponds to the wavenumber. The dispersion analysis of the dynamic response will be explained in the next section.

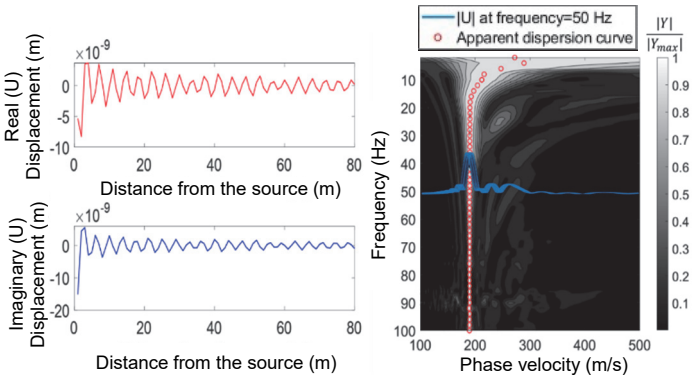

Fig. 3 (a) An example of simulated frequency response, $U(f, x_n)$, at f = 50 Hz, including the real part and imaginary part; (b) The corresponding normalized amplitude spectrum ($|Y| / |Y_{\max}|$)

2.3 Apparent Dispersion Curves

In the MASW testing, the wavefield is sampled and denoted as $u(t_m, x_n)$, where m and n represent the data index in time and space, respectively. To analyze the dispersion characteristics of the wavefield, several algorithms have been developed, such as the frequency-wavenumber (*f-k)* transform (Yilmaz 1987), slowness-

frequency (*p*-ω) transform (McMechan and Yedlin 1981), phase shift method (Park *et al.* 1998), and the cylindrical beamformer transform (Zywicki and Rix 2005). In the nature of "apparent" or "effective" dispersion curve, none of these algorithms is necessarily superior to the others. In fact, except for the cylindrical beamformer, other wavefield transform methods are mathematically and physically equivalent (Lin and Chang 2004) although the algorithm in the phase-shift method is mostly adopted. In general, the first step in the dispersion analysis of seismic data is to take the Fourier transform of the multi-station data $u(t_m, x_n)$ with respect to time to find the seismic data in the frequency domain $U(f, x_n)$.

$$U(f,\ x_n) = \sum_{m=0}^{M-1} u(t_m,\ x_n) \exp(-j2\pi f x_n) \tag{1}$$

where f is the frequency ($\omega = 2\pi f$) and M is the total number of data points in time; m and n are data points indices for time t and offset x. In the synthetic data described in the previous section, $U(f, x_n)$ is the computed frequency response. Hence, we can directly proceed to the second step in the dispersion analysis, which, in this study, is to take the Fourier transform with respect to space.

$$W(f,\ k) = \sum_{n=0}^{N-1} U(f,\ x_n) \exp(-j2\pi k x_n) \tag{2}$$

where k is the wavenumber. Equations (1) and (2) combined are basically the same as the *f-k* transform. To facilitate common spectral visualization in the frequency-phase velocity domain, we replace the wavenumber k by $k = 2\pi f/v$ so that Eq. (2) becomes

$$Y(f,\ v) = \sum_{n=0}^{N-1} W(f,\ x_n) \exp\left(-j\frac{2\pi f}{v} x_n\right) \tag{3}$$

where v is the phase velocity. Equation (3) is equivalent to the phase-shift method. The amplitude spectrum of $Y(f, v)$ gives the dispersion image commonly seen in the literature. In the numerical implementation, the frequency and phase velocity intervals (resolutions) can be arbitrarily chosen. An example is illustrated in Fig. 3(b). Figure 3(a) is the frequency response at $f = 50$ Hz. Applying Eq. (3), the amplitude spectrum of Y for the 50 Hz component is shown by a line plot at the elevation of 50 Hz. Results from simulations of many frequency responses would then be represented by the dispersion image. The peaks of the dispersion image correspond to the apparent dispersion curve (dominant phase velocity for each frequency). The apparent dispersion curves from different velocity profiles would be examined to study their behavior in relation to the type of velocity profile.

2.4 Simplified Inversion Method

The last step of a complete surface wave testing is to invert the V_S profile from the experimental dispersion curve. In the current MASW practice, we try to arrange the seismic survey and analysis so that the fundamental mode can be extracted from the apparent dispersion curve (*i.e.,* the entire apparent dispersion curve or part of it below certain frequency). The main objective of this study is to reveal the behavior of apparent dispersion curve so that a more compatible inversion scheme may be devised. Therefore, a rigorous inversion is beyond the scope of this study. However, the simplified inversion method (SIM) will be examined as an extension of the behavior of surface wave dispersion. It can also shed some light on setting up more reasonable initial V_S profile for a rigorous inversion.

The apparent dispersion curve in terms of phase velocity (v) *vs.* wavelength (λ) was directly transformed to shear wave velocity (V_S) *vs.* depth (D) using the simplified inversion method (SIM) proposed by Pelekis and Athanasopoulos (2011), evolved from the original Satoh *et al.* (1991) method. The dispersion curve (v *vs.* λ) is first transformed to an apparent velocity ($\bar{V}_R$) vs. depth (D) by converting the wavelength values to the equivalent depths, $D = \alpha_z\lambda$ and taking the apparent velocity $\bar{V}_R = v$. According to Pelekis and Athanasopoulos (2011), the value of depth conversion factor (α_z) depends on the Poisson's ratio and the type of dispersion (*i.e.,* normal *vs.* inverse dispersion). For the normal dispersive case, α_z increases from 0.3 to 0.85 for Poisson's ratio ranging from 0 to 0.5. In the case of inverse dispersion (*i.e.,* phase velocity decreases with wavelength), α_z becomes independent of the Poisson's ratio, with an average value of $\alpha_z = 0.45$. Hence, there is no universal rule for choosing α_z, and different values have been adopted in the literatures (*e.g.,* Tamrakar and Luke 2013; Moon *et al.* 2017). Since the SIM is more of a qualitative approach, $\alpha_z = 0.5$ was chosen for equivalent depth conversion. In a more rigorous inversion, different values can be tested for minimizing the data misfit.

After equivalent depth conversion, the apparent phase velocity $\bar{V}_R$ *vs.* D was approximated by a best fit multilinear curve, in which each linear segment is assumed to correspond to a separate soil layer, as illustrated in Fig. 4. The Rayleigh wave velocity, V_R, for each individual layer was then calculated using the following two equations for the case of increasing or decreasing velocity with depth, respectively.

$$V_{Rn} = \frac{\bar{V}_{Rn} D_n - \bar{V}_{Rn-1} D_{n-1}}{D_n - D_{n-1}} \tag{4}$$

$$V_{Rn} = \frac{D_n - D_{n-1}}{\dfrac{D_n}{\bar{V}_{Rn}} - \dfrac{D_{n-1}}{\bar{V}_{Rn-1}}} \tag{5}$$

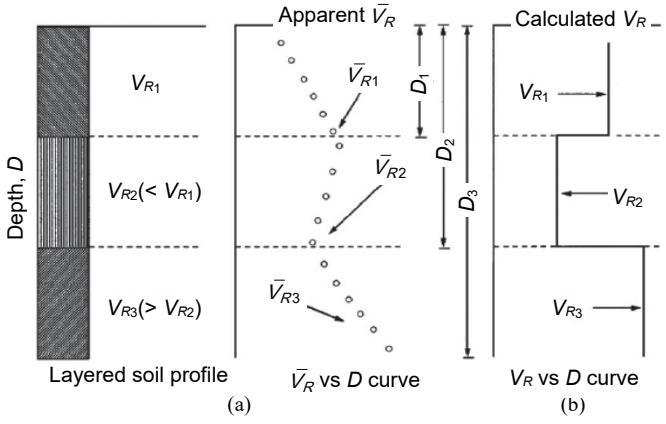

Fig. 4 Simplified inversion scheme for determining Rayleigh wave velocity of each layer: (a) The assumed 3-layer V_R velocity profile and the corresponding dispersion curve with wavelength transformed to equivalent depth (D); (b) The estimated V_R profile using Eq. (4) (Satoh *et al.* 1991)

where the subscript n and $n-1$ represent the depth index at the lower and upper interface of the n^{th} layer, respectively. The Rayleigh wave velocity of each layer is finally converted to the shear wave velocity by $V_S = \alpha_v V_R$. The velocity conversion factor α_v also depends on the Poisson's ratio (*e.g.,* Richart *et al.* 1970), but varies in a small range around 1.1. Hence, $\alpha_v = 1.1$ was taken in this study.

In the context of SASW method, a single synthesized (averaged) apparent dispersion curve is obtained that enables the application of SIM. On the contrary, multiple separate pieces of dispersion curves may be obtained in the MASW method. The MASW method offers robust and objective dispersion analysis, and allows separation of multiple modes in complex ground conditions when the receiver array is long enough. For a single frequency (or wavelength), there may be more than one significant mode (phase velocity). How the SIM can be adapted and applied in this scenario will be discussed below.

3. RESULTS AND DISCUSSIONS

The following discussion will focus on the apparent dispersion curves emerged from the wavefield transformation of the multi-station data, as opposed to the theoretical modal dispersion curves. MASW has the advantage of efficient, robust, and objective dispersion analysis. With an enough long geophone spread, it is possible to extract the fundamental mode from other possible higher modes, hence justifying the fundamental-mode inversion in current practice. However, accurate and wide frequency range of fundamental-mode dispersion curve is not guaranteed in every survey. The following discussion will examine the actual dispersion behavior, *i.e.,* the pattern of the apparent dispersion curve and characteristics of dispersion image ($|Y(f, v)|$), of the four distinct types of velocity profiles.

3.1 Normal Velocity Profile (Increasing V_S with Depth)

Figure 5 shows the results for the case of regular V_S profiles, in which V_S increases with depth. These include two-layer models with different velocity contrast and a three-layer model. As shown in Fig. 5(a) and expected, the fundamental mode dominates in the entire frequency range, *i.e.,* high amplitudes of the dispersion

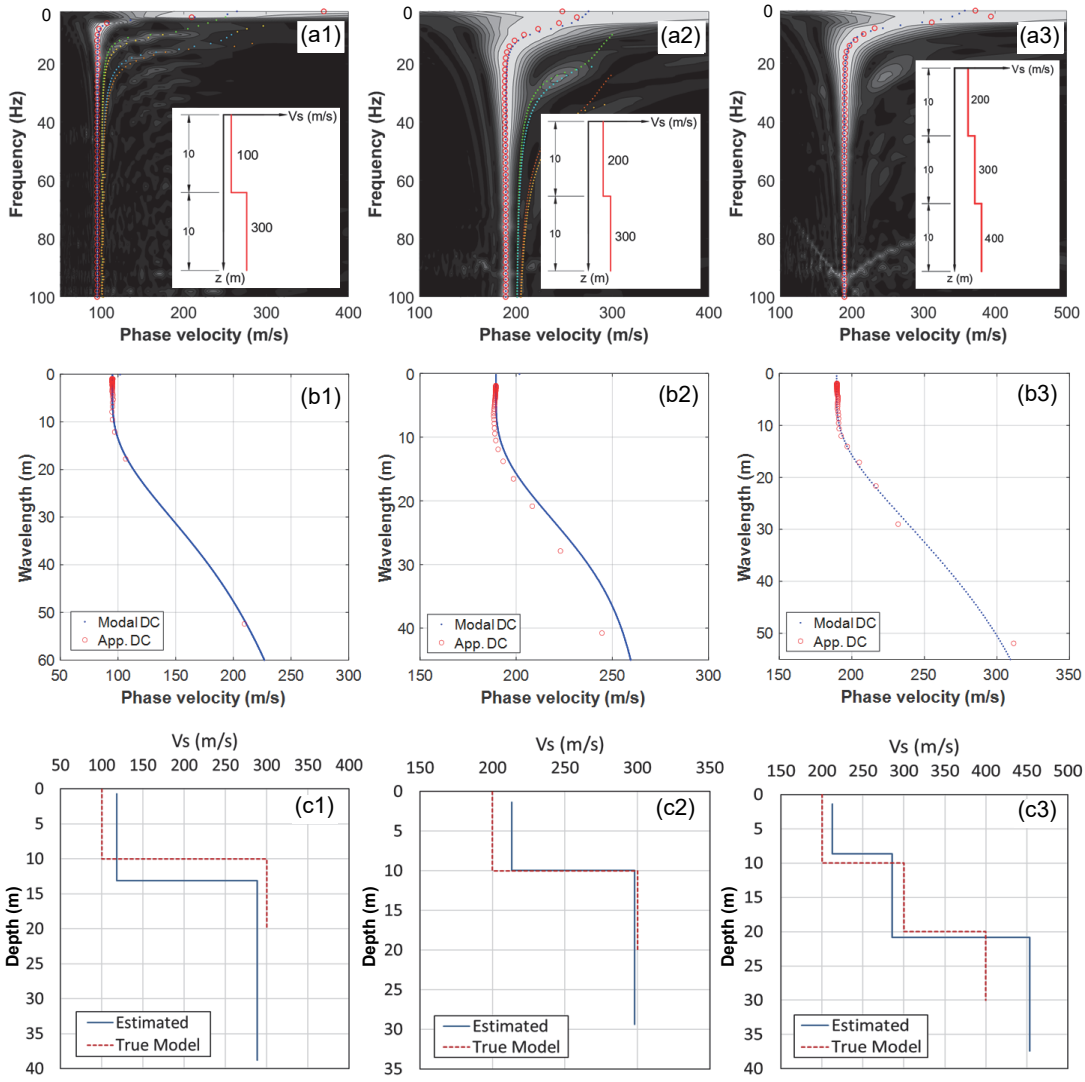

Fig. 5 Results of normal velocity profile: (a) dispersion image for each velocity profile shown in the inserted box. Dotted lines represent the theoretical modal dispersion curve, and circles are the apparent dispersion curve (peaks of the dispersion image); (b) comparison between the apparent dispersion curve (App. DC) and theoretical modal dispersion curve (Modal DC) in the wavelength-phase velocity domain; (c) comparison between the estimated V_S profile by SIM and the true velocity model

spectrum are basically on the fundamental mode. Some higher modes have significant contributions in certain frequency range. This is more obvious in the two-layer model with larger velocity contrast (Fig. 5(a1)). The apparent dispersion curve corresponding to the peaks of the dispersion image basically follows the fundamental mode, as shown in Fig. 5(b). The phase velocity monotonically increases with wavelength since *Vs* increases with depth. Some discrepancy from the theoretical fundamental mode at longer wavelength (lower frequency) is attributed to the near field and truncation effects of the limited wavefield acquired by the 48-channel geophone array. In any case, Fig. 5(c) shows that the SIM-estimated *Vs* profiles match very well with the true velocities.

3.2 Inverse Velocity Profile (Decreasing *Vs* with Depth)

Similar to Fig. 5, Fig. 6 presents the results for the case of inverse velocity profile. Beyond some cutoff frequency as shown in Fig. 6(a) or below some cutoff wavelength as shown in Fig. 6(b), the apparent dispersion curve would jump from the fundamental mode to higher mode(s). In minor inverse velocity profile, where the lower-half space velocity is not significantly lower than the top layer (Fig. 6(a1)), the first higher mode is very close to the fundamental mode. As such, the higher mode cannot be well separated from the fundamental mode, as shown in Figs. 6(a1) and 6(b1). By examining all results of inverse velocity profiles, it can be found that the cutoff wavelength is near the top of the lower half space. This means that only when the wavelength reaches the lower half space would the fundamental mode become the dominant mode. While the two-layer case (Fig. 6(a2) and 6(b2)) shows one clear higher mode, the three-layer case contains several mode jumps. These mode jumps are not very apparent because pairs of theoretical higher modes show mode kissing at the frequency of the mode jumping. Therefore, the apparent dispersion curve looks like a single continuous curve, especially in the frequency-phase velocity domain (Fig. 6(a3)). For the case shown in Fig. 6(b2), the SIM procedure cannot be applied because the apparent dispersion curve does not appear as a continuous curve. In this case, we

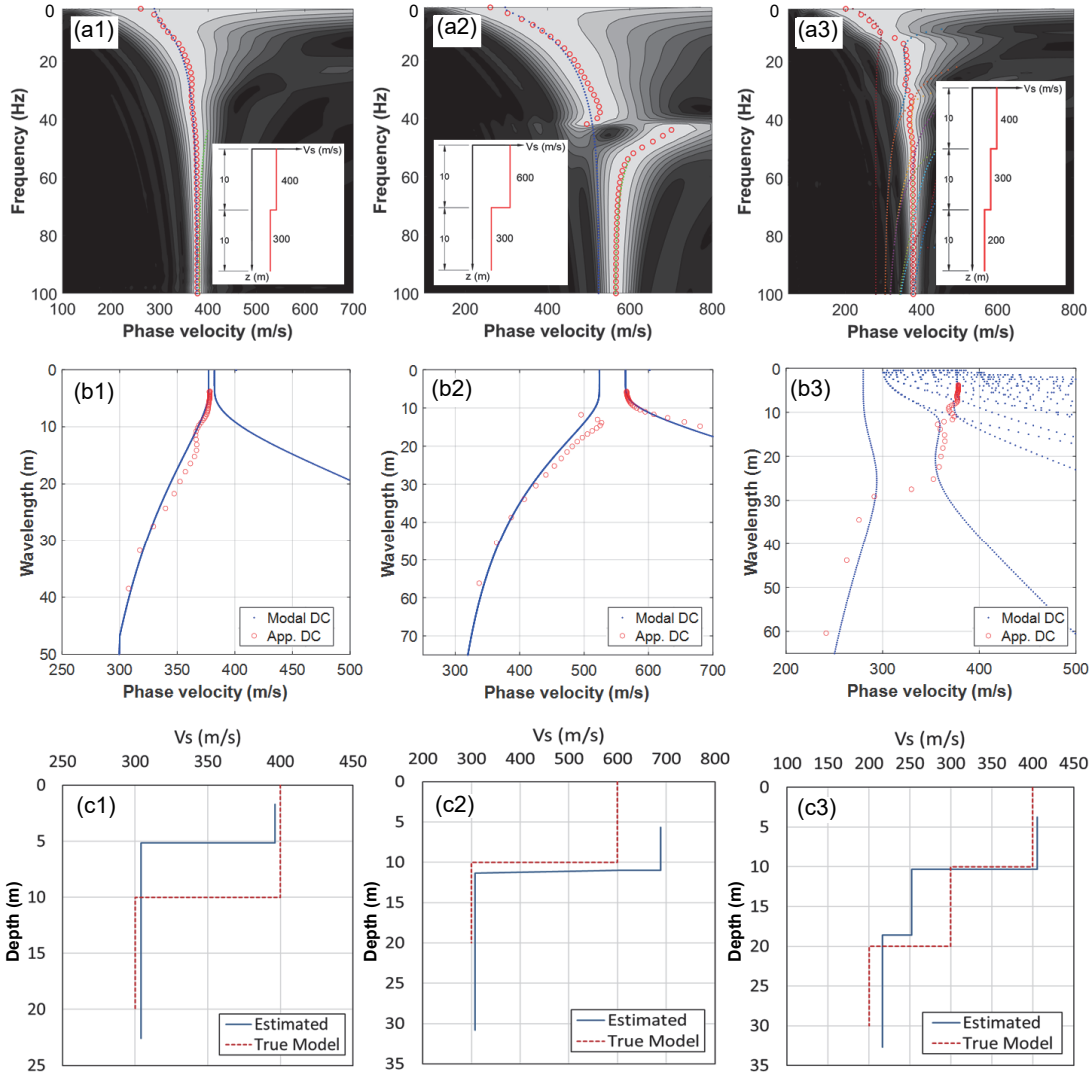

Fig. 6 Results of inverse velocity profile: (a) dispersion image for each velocity profile shown in the inserted box. Dotted lines represent the theoretical modal dispersion curve, and circles are the apparent dispersion curve (peaks of the dispersion image); (b) comparison between the apparent dispersion curve (App. DC) and theoretical modal dispersion curve (Modal DC) in the wavelength-phase velocity domain; (c) comparison between the estimated *Vs* profile by SIM and the true velocity model

proposed to discard the higher mode at overlapping frequencies (wavelengths) and extend the SIM to the piece-wise continuous dispersion curve. Another modification to the SIM is needed to obtain better results. Since the apparent dispersion curve would approach the fundamental mode only when the wavelength is larger than the depth of the top of the lower half space, using an equivalent depth conversion factor $\alpha_z = 0.5$ or even higher values from the literatures would significantly underestimate the depth to the lower half space. We therefore propose to use $\alpha_z = 1.0$ in the small wavelength range where higher modes dominate because the cutoff wavelength is approximately equal to the depth to the lowest half space. As a result of this modification, the SIM would provide better estimated V_S profile, as shown in Figs. 6(c2) and (c3). Because the higher mode cannot be clearly identified for the case shown in Fig. 6(a1), the standard SIM would result in significant underestimation of the depth to the lower half space, as shown in Fig. 6(c1). Due to the mode jumping, the apparent dispersion curve of the inverse dispersion is not as smooth as that of the normal dispersion. Consequently, the uncertainty of the SIM estimation in the inversion dispersion case is generally higher than that in the normal dispersion case.

3.3 Velocity Profile of Sandwiched Stiff/Soft Layer

Results for the case of sandwiched stiff layer are shown in Fig. 7. All results are basically dominated by the fundamental mode as in the case of normal dispersion. The apparent dispersion curve becomes concave due to the existence of the embedded stiff layer, as shown in Figs. 7(a) and 7(b). However, it is noted that the near-field effect is more pronounced in the case of sandwiched stiff layer, causing more discrepancy from the theoretical fundamental mode at long wavelengths. Furthermore, when the velocity contrast becomes larger, as shown in Fig. 7(a2) and near the vertex, the apparent dispersion curve is further away from the fundamental mode. For frequencies near the vertex, the apparent dispersion curve appears to be of mixed modes. When the stiff layer becomes

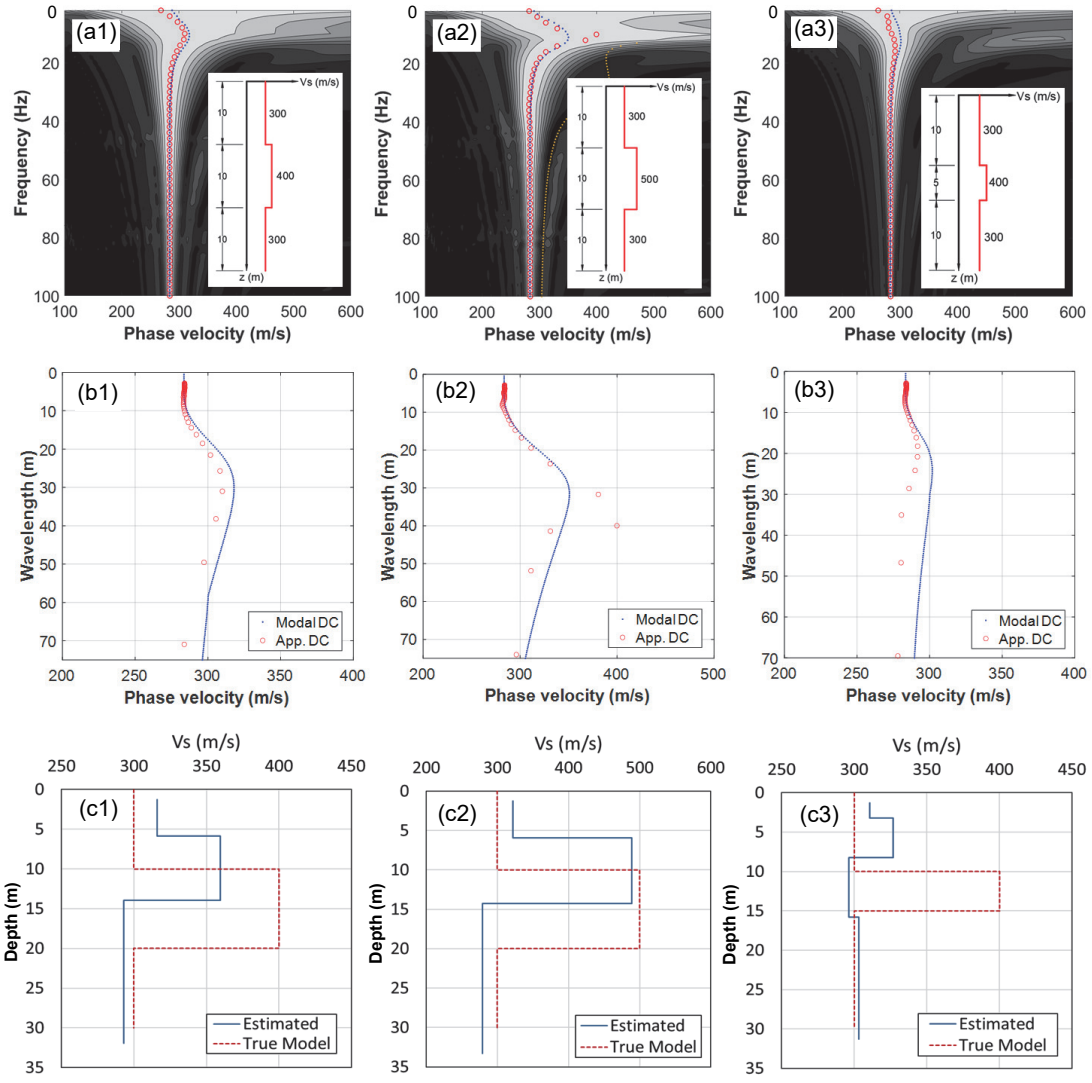

Fig. 7 Results of sandwiched stiff layer: (a) dispersion image for each velocity profile shown in the inserted box. Dotted lines represent the theoretical modal dispersion curve, and circles are the apparent dispersion curve (peaks of the dispersion image); (b) comparison between the apparent dispersion curve (App. DC) and theoretical modal dispersion curve (Modal DC) in the wavelength-phase velocity domain; (c) comparison between the estimated V_S profile by SIM and the true velocity model

thinner, as shown in Fig. 7(a3), the apparent dispersion curve is less sensitive to the stiff layer and the near-field effect seems even more pronounced. The estimated V_S profiles using the SIM are shown in Fig. 7(c). The embedded stiff layer can be detected but contains larger errors due to the near-field effect. This indicates potential problems of fundamental-mode inversion, because a reliable fundamental-mode dispersion curve may not be obtained from the apparent dispersion curve as indicated by these examples.

Figure 8 presents the results for the case of sandwiched soft layer. Similar to the inverse velocity profile case, higher modes dominate when the wavelength is smaller than the depth to the bottom layer. The transition from one mode to another may not have a fixed pattern; hence assigning the mode number to the dominant higher modes is impossible. When the velocity contrast becomes more significant, as in Fig. 8(a1), or the embedded soft layer becomes thinner, as in Fig. 8(a3), a local jump to a higher mode with much higher phase velocity may occur. In these cases, the lower bound of the apparent dispersion curve is taken from SIM analysis. When the velocity contrast is not significant, the apparent dispersion curve appears more like a single continuous curve because of the higher mode transition. As in the inverse velocity profile, the equivalent depth conversion factor was taken as $\alpha_z = 1.0$ for higher modes at smaller wavelengths. Figure 8(c) shows the estimated V_S profiles using the SIM. The embedded soft layer can be clearly identified and the depth to the soft layer is accurate using the modified equivalent depth conversion factor. However, the error is larger beneath the top layer. More advanced inversion is necessary to better recover this type of velocity profile. Considering that the fundamental mode appears only in the wavelength greater than the depth to the low half space, the advanced inversion should be based on the apparent dispersion curve or dispersion image, not the fundamental mode.

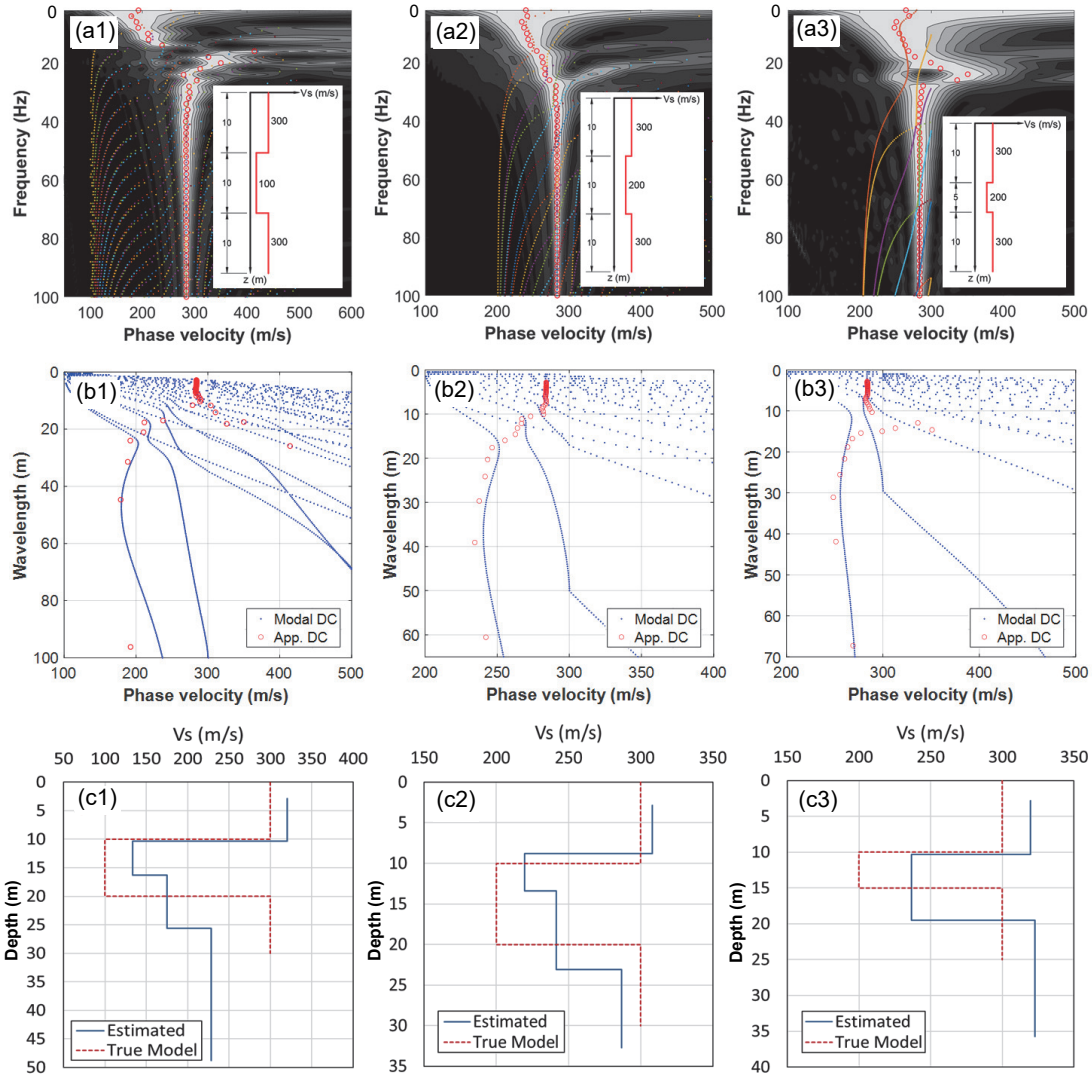

Fig. 8 Results of sandwiched soft layer: (a) dispersion image for each velocity profile shown in smaller box (dotted lines represents the theoretical modal dispersion curve, and circles are the apparent dispersion curve (peaks of the dispersion image); (b) the comparison between the apparent dispersion curve and theoretical modal dispersion curve in the wavelength-phase velocity domain; (c) comparison between the estimated V_S profile by SIM and the true velocity model

3.4 Complex 4-Layer Model

The complex 4-layer model is the most sophisticated one in this study. It is by no means to represent the actual field condition. It can shed some light on the dispersion behavior in a situation that is often encountered in the field -- an embedded soft layer in a profile that the shear wave velocity otherwise increases with depth. Results are shown in Fig. 9. When the soft layer is not significantly softer than the top layer, as in Fig. 9(a1) with only 10% difference, the apparent dispersion curve appears to follow the fundamental mode in the entire frequency range. However, a close comparison with the theoretical modal dispersion curves reveals that a few higher modes are very close to the fundamental mode in the higher frequency range and the apparent dispersion curve below 5 m wavelength actually corresponds to higher modes. As the velocity contrast between the top layer and the embedded soft layer becomes more significant, as shown in Fig. 9(a3), the apparent dispersion curve clearly jumps to higher modes at wavelength smaller than the depth to the bottom of the soft layer, as can be observed in Fig. 9(b3). Comparing to Fig. 9(a3), Fig. 9(a2) represents the case with a thinner top layer while Fig. 9(a4) represents the case with a thinner soft layer. Both cases have the same depth to the bottom of the soft layer (6 m), and hence the fundamental mode dominates at wavelength greater than 6 m. Figure 9(c) shows the estimated Vs profiles using the SIM. Again, using the apparent dispersion curve and SIM, the embedded soft layer can be detected except for the case in Fig. 9(a1), in which the velocity of embedded soft layer is very close to the top layer. Similar to the sandwiched soft layer, the estimation error is significant at depth below the stiffer top layer. The case in Fig. 9(a1) is very close to the condition of regular velocity profile, in which the SIM works better. However, comparing Fig. 9(c1) with Fig. 5(c1), larger estimation errors can be observed at depth below 10 m because of the existence of a mild soft layer. This result implies that the SIM is not a rigorous inversion and its reliability is dependent on the type of velocity profile.

Comparing all the cases in Fig. 9 shows distinct dispersion images and patterns of dominant higher modes in response to different layer thickness and velocity. The difference in their dispersion images is so remarkable that it is not unreasonable to think that future inversion based on the dispersion image may significantly improve the accuracy and resolution. This type of velocity profile also shows that it is not possible to identify the exact mode numbers of the dominant higher modes. Performing inversion based on only the fundamental mode means that a significant amount of dispersion curve data will be discarded. This will decrease the measurement sensitivity to the variation of velocity

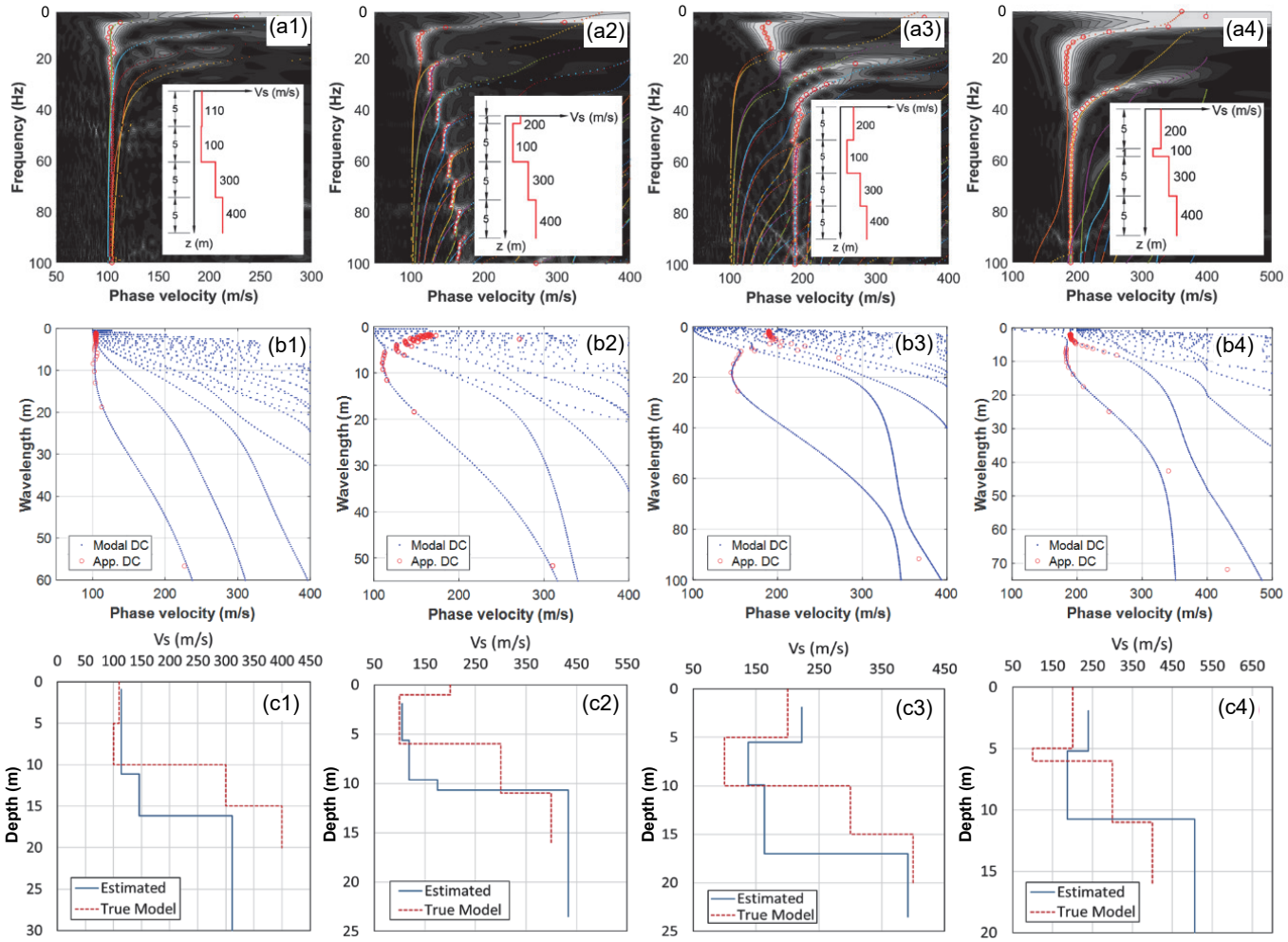

Fig. 9 Results of complex velocity profile: (a) dispersion image for each velocity profile shown in the inserted box. Dotted lines represent the theoretical modal dispersion curve, and circles are the apparent dispersion curve (peaks of the dispersion image); (b) comparison between the apparent dispersion curve (App. DC) and theoretical modal dispersion curve (Modal DC) in the wavelength-phase velocity domain; (c) comparison between the estimated Vs profile by SIM and the true velocity model

profile. Therefore, it is believed that working on apparent dispersion curve or dispersion image is imperative to further improve the reliability of the MASW method.

4. CONCLUSIONS AND SUGGESTIONS

Current practice of the MASW method mainly focuses on the fundamental mode, counting on the ability of multi-station data to separate different participating modes and extract the fundamental mode for inversion. Emphasized in this study is the potential difference between the theoretical dispersion curves, intrinsic to earth profile, and the experimental apparent dispersion curve, dependent also on the configuration of receiver array. Simulating modal and apparent dispersion curves for the four distinct types of V_S profiles reveal their different dispersion characteristics and behavior of apparent dispersion curve. Several findings can be drawn from these results.

1. If there is no intermediate layer which is softer than the surface layer, *e.g.,* normal velocity profile or sandwiched stiff layer, the apparent dispersion curve is dominated by the fundamental mode. However, different levels of discrepancy between the apparent and fundamental-mode dispersion curves can be observed due to the near-field effect and sometimes due to the mixed modes at certain frequencies.
2. If the surface layer is not the softest layer, the apparent dispersion curve is dominated by the higher modes at relatively high frequencies (low wavelengths). It can be inferred from various simulations that the transition from the fundamental-mode dominance to higher-mode dominance is at the wavelength approximately equal to the depth to the low half space (*i.e.,* in the inverse velocity profile) or the low half space below the softest layer (*i.e.,* in cases with embedded soft layer). Depending on the location of the softest layer, the minimum wavelength of the measurable fundamental mode may be quite large. Performing inversion based on only the fundamental mode means that a significant amount of apparent dispersion curve data may have to be discarded.
3. Depending on the spread length of receivers, and velocity contrast and thickness of the soft layer, the fundamental mode may not be well separated from higher modes, and the apparent dispersion curve may appear as a single continuous curve. Hence, sometimes it is not easy to clearly define the frequency range of the fundamental mode.
4. In the case of higher-mode dominance, there is no fixed pattern as to which higher mode would dominate the sequence of mode jumping. Therefore, definite assignment of mode numbers in multi-mode inversion is unlikely.

These new observations lead to some potential pitfalls of the MASW fundamental-mode inversion. Our study has further shown the remarkable difference in dispersion images and patterns of dominant higher modes in response to different velocity profiles. The simplified inversion method (SIM) has been modified to deal with the multiple dominant modes. The SIM can correctly detect the embedded soft layer and the type of velocity profile; however, its accuracy is not good across different type of velocity profiles. Hence, it is suggested that more rigorous inversion based on apparent dispersion curve or dispersion spectrum image is imperative to further improve the reliability of the MASW method.

ACKNOWLEDGEMENTS

The authors would like to thank both Dr. Feng Zhu and Dr. Ru Tian for their helps on issues related to the calculation of the dispersion curve.

FUNDING

This work is funded by the Ministry of Science and Technology, Taiwan, under project number 108-2625-M-009.

DATA AVAILABILITY

This study does not generate new data and/or new computer codes.

CONFLICT OF INTEREST STATEMENT

The authors declare that they have no known conflict of interests or personal relationships that could have appeared to influence the work reported in this paper.

REFERENCES

Al-Khoury, R., Scarpas, A., Kasbergen, C., and Blaauwendraad, J. (2001). "Spectral element technique for efficient parameter identification of layered media. I. Forward calculation." *International Journal of Solids and Structures*, **38**, 1605-1623. https://doi.org/10.1016/S0020-7683(00)00112-8

Alkasawneh, W., Pan, E., Han, F., Zhu, R., and Green, R. (2007). "Effect of temperature variation on pavement responses using 3D multilayered elastic analysis." *International Journal of Pavement Engineering*, **8**(3), 203-212. https://doi.org/10.1080/10298430601116741

Di Benedetto, H., Doanh, T., Geoffroy, H., and Sauzeat, C. (Eds.) (2003). *Deformation Characteristics of Geomaterial*, A.A. Balkema Publishers, Tokyo, 1425 p.

Foti, S. (2003). "Small-strain stiffness and damping ratio of Pisa clay from surface wave tests." *Géotechnique*, **53**(5), 1751-7656. https://doi.org/10.1680/geot.2003.53.5.455

Ganji, V., Gucunski, N., and Nazaraian, S. (1998). "Automated inversion procedure for spectral analysis of surface waves." *Journal of Geotechnical and Geoenvironmental Engineering*, ASCE, **124**(8), 757-770. https://doi.org/10.1061/(ASCE)1090-0241(1998)124:8(757)

Haskell, N.A. (1953). "The dispersion of surface waves on multilayered media." *Bulletin of the Seismological Society of America*, **43**(1), 17-34. https://doi.org/10.1785/BSSA0430010017

Heisey, J.S., Stokoe, K.H., and Meyer, A.H. (1982). "Moduli of pavement systems from spectral analysis of surface waves." *Transportation Research Record*, **852**(22-31), 147.

Joh, S.H. (1996). *Advances in the Data Interpretation Techniques for Spectral Analysis of Surface Waves (SASW) Measurement*. Ph.D. Dissertation, University of Texas at Austin.

Kausel, E. and Roesset, J.M. (1981). "Stiffness matrices for layered soils." *Bulletin of the Seismological Society of America*, **71**(6), 1743-1761. https://doi.org/10.1785/BSSA0710061743

Lin, C.P. and Chang, T.S. (2004). "Multi-station analysis of surface wave dispersion." *Soil Dynamics and Earthquake Engineering*, **24**, 877-886.

https://doi.org/10.1016/j.soildyn.2003.11.011
Lin, C.P., Chang, C.C., and Chang, T.S. (2004). "The use of MASW method in the assessment of soil liquefaction potential." *Soil Dynamics and Earthquake Engineering*, **24**(9-10), 689-698. https://doi.org/10.1016/j.soildyn.2004.06.012
Lin, C.P., Lin, C.H., and Chien, C.J. (2017). "Dispersion analysis of surface wave testing-SASW vs. MASW." *Journal of Applied Geophysics*, **143**, 223-230. http://dx.doi.org/10.1016/j.jappgeo.2017.05.008
Liu, H. and Pan, E. (2018). "Time-harmonic loading over transversely isotropic and layered elastic half spaces with imperfect interfaces." *Soil Dynamics and Earthquake Engineering*, **107**, 35-47. https://doi.org/10.1016/j.soildyn.2018.01.003
Liu, H., Pan, E., and Cai, Y. (2018). "General surface loading over layered transversely isotropic pavements with imperfect interfaces." *Advances in Engineering Software*, **115**, 268-282. https://doi.org/10.1016/j.advengsoft.2017.09.009
Lu, Y., Cao, Y., McDaniel, J.G., and Wang, M.L. (2015). "Fast inversion of air-coupled spectral analysis of surface wave (SASW) using in situ particle displacement." *ISPRS International Journal of Geo-Information*, **4**(4), 2619-1637. https://doi.org/10.3390/ijgi4042619
Lucena, R.F. and Taioli, F. (2014). "Rayleigh wave modeling: a study of dispersion curve sensitivity and methodology for calculating an initial model to be included in inversion algorithm." *Journal of Applied Geophysics*, **108**, 140-151. http://dx.doi.org/10.1016/j.jappgeo.2014.07.007
McMechan, G.A. and Yedlin, M.J. (1981). "Analysis of dispersive waves by wave field transformation." *Geophysics*, **46**, 869-874. https://doi.org/10.1190/1.1441225
Moon, S.-W., Hayashi, K., and Ku, T. (2017). "Estimating spatial variations in bedrock depth and weathering degree in decomposed granite from surface waves." *Journal of Geotechnical and Geoenvironmental Engineering*, ASCE, **143**(7), 04017020. https://doi.org/10.1061/(ASCE)GT.1943-5606.0001679
Olafsdottir, E.A., Erlingsson, S., and Bessason, B. (2018). "Tool for analysis of multichannel analysis of surface waves (MASW) field data and evaluation of shear wave velocity profiles of soils." *Canadian Geotechnical Journal*, **55**(2), 217-233. https://doi.org/10.1139/cgj-2016-0302
Park, C.B., Miller, R.D., and Xia, J. (1998). *Imaging Dispersion Curves of Surface Waves on Multi-Channel Record*. SEG Technical Program Expanded Abstracts, 1377-1380. http://dx.doi.org/10.1190/1.1820161
Park, C.B., Miller, R.D., and Xia, J. (1999). "Multichannel analysis of surface waves." *Journal of Geophysics*, 800-808. https://doi.org/10.1190/1.1444590
Park, C. and Carnevale, M. (2010). "Optimum MASW survey-revisit after a decade of use." *Proceeding of GeoFlorida 2010: Advances in Analysis, Modeling & Design*, Florida, 1303-1312.
Pelekis, P.C. and Athanasopoulos, G.A. (2011). "An overview of surface wave methods and a reliability study of a simplified inversion technique." *Soil Dynamics and Earthquake Engineering*, **31**, 1654-1668. http://dx.doi.org/10.1016/j.soildyn.2011.06.012
Richart, Jr., F.E., Hall, Jr., J.R., and Woods, R.D. (1970), *Vibrations of Soils and Foundations*, Prentice Hall, Englewood Cliffs, New Jersey, 414 p.
Roesset, J.M. and Shao, K. (1985). "Dynamic interpretation of dynaflect and falling weight deflectometer tests." *Transportation Research Record*, 1022, 7-16.
Satoh, T., Poran, C.I., Yamagata, K., and Rondriquez, J.A. (1991). "Soil profiling by spectral analysis of surface waves." *Proceedings of the Second International Conference on Recent Advances in Geotechnical Earthquake Engineering and Soil Dynamics*, St. Louis, 1429-1434.
Stokoe, K.H., John, S.H., and Woods, R.D. (2004). "Some contributions of in situ geophysical measurements to solving geotechnical engineering problems." *Proceedings of 2nd International Conference on Site Characterization*, Porto, Portugal, **1**, 97-132.
Tamrakar, P. and Luke, B. (2013). "Feasibility of approximating depth to shallow bedrock directly from the Rayleigh wave dispersion curve." *Geotechnical Testing Journal*, **36**(6), 882-890. https://doi.org/10.1520/GTJ20120080
Thomson, W.T. (1950). "Transmission of elastic waves through a stratified solid medium." *Journal of Applied Physics*, **21**(2), 89-93. https://doi.org/10.1063/1.1699629
Tokimatsu, K. (1995). "Geotechnical site characterization using surface waves." *Proceeding of 1st International Conference on Earthquake Geotechnical Engineering*, Tokyo, Japan, 1333-1368.
Xia, J., Miller, R.D., and Park, C.B. (1999). "Estimation of near-surface shear-wave velocity by inversion of Rayleigh waves." *Geophysics*, **64**, 691-700. https://doi.org/10.1190/1.1444578
Xia, J., Miller, R.D., Park, C.B., and Tian, G. (2003). "Inversion of high frequency surface waves with fundamental and higher modes." *Journal of Applied Geophysics*, **52**(1), 45-57. https://doi.org/10.1016/S0926-9851(02)00239-2
Yilmaz, O. (1987). *Seismic Data Processing*. Tulsa, Oklahoma: Society of Exploration Geophysicists.
Zhou, J., Pan, E., and Bevis, M. (2021). "A point dislocation in a layered, transversely isotropic and self-gravitating Earth. Part IV: Exact asymptotic solutions of dislocation Love numbers for the special case of isotropy." *Geophysical Journal International*, **225**(1), 664-683. http://dx.doi.org/10.1093/gji/ggz110
Zywicki, D.J. and Rix, G.J. (2005). "Mitigation of near-field effects for seismic surface wave velocity estimation with cylindrical beam formers." *Journal of Geotechnical and Geoenvironmental Engineering*, ASCE, **131**(8), 970-977. https://doi.org/10.1061/(ASCE)1090-0241(2005)131:8(970)